NEOPLASIA
www.neoplasia.com

Volume 14 Number 6 June 2012 pp. 451–462 451

Combined *In Vivo* Molecular and Anatomic Imaging for Detection of Ovarian Carcinoma–Associated Protease Activity and Integrin Expression in Mice[1,2]

Harvey H. Hensley[*,3], Navid A. Roder[*,3], Shane W. O'Brien[†], Laura E. Bickel[†], Fang Xiao[†], Sam Litwin[‡] and Denise C. Connolly[†]

*Biological Imaging Facility, Fox Chase Cancer Center, Philadelphia, PA; [†]Women's Cancer Program, Fox Chase Cancer Center, Philadelphia, PA; [‡]Biostatistics and Bioinformatics Facility, Fox Chase Cancer Center, Philadelphia, PA

Abstract

Most patients with epithelial ovarian cancer (EOC) experience drug-resistant disease recurrence. Identification of new treatments is a high priority, and preclinical studies in mouse models of EOC may expedite this goal. We previously developed methods for magnetic resonance imaging (MRI) for tumor detection and quantification in a transgenic mouse model of EOC. The goal of this study was to determine whether three-dimensional (3D) fluorescence molecular tomography (FMT) and fluorescent molecular imaging probes could be effectively used for *in vivo* detection of ovarian tumors and response to therapy. Ovarian tumor–bearing Tg*MISIIR-TAg* mice injected with fluorescent probes were subjected to MRI and FMT. Tumor-specific probe retention was identified *in vivo* by alignment of the 3D data sets, confirmed by *ex vivo* fluorescent imaging and correlated with histopathologic findings. Mice were treated with standard chemotherapy, and changes in fluorescent probe binding were detected by MRI and FMT. Ovarian tumors were detected using probes specific for cathepsin proteases, matrix metalloproteinases (MMPs), and integrin $\alpha_v\beta_3$. Cathepsin and integrin $\alpha_v\beta_3$ probe activation and retention correlated strongly with tumor volume. MMP probe activation was readily detected in tumors but correlated less strongly with tumor volume. Tumor regression associated with response to therapy was detected and quantified by serial MRI and FMT. These results demonstrate the feasibility and sensitivity of FMT for detection and quantification of tumor-associated biologic targets in ovarian tumors and support the translational utility of molecular imaging to assess functional response to therapy in mouse models of EOC.

Neoplasia (2012) 14, 451–462

Introduction

Epithelial ovarian cancer (EOC) is the most common form of ovarian cancer. Localized ovarian tumors are typically associated with nonspecific symptoms, and the majority of women present with disseminated peritoneal disease [1]. Although most patients respond well to aggressive surgical debulking and combination chemotherapy consisting of platinum and taxane, the majority experience disease recurrence and ultimately drug resistance, making EOC the most lethal of the gynecologic malignancies [1]. Hence, there is a critical need to identify therapeutics that target pathways specific to ovarian cancer tumor progression.

Targeting single molecules or pathways in tumor cells may initially show efficacy; but these strategies may ultimately fail because of the development of drug resistance based on mutation of the target, compensatory

Abbreviations: EOC, epithelial ovarian cancer; FMT, fluorescence molecular tomography; MMP, matrix metalloproteinase; MOVCAR, murine ovarian carcinoma; AMIDE, A Medical Imaging Data Examiner; ROI, region of interest

Address all correspondence to: Denise C. Connolly, PhD, or Harvey H. Hensley, PhD, 333 Cottman Ave, Philadelphia, PA 19111. E-mail: Denise.Connolly@fccc.edu, Harvey.Hensley@fccc.edu

[1]This project was supported by the Fox Chase Cancer Center (FCCC) – University of Pennsylvania Ovarian Cancer SPORE CA083638, the FCCC Keystone Initiative in Personalized Risk and Prevention, the Bucks County Board of Associates, The Teal Tea Foundation, and the FCCC Laboratory Animal, Biomedical Imaging, Histopathology and Biostatistics Facilities. D.C.C. is supported by grants CA136596, CA151374, CA083638, and CA006927 from the National Cancer Institute.

[2]This article refers to supplementary materials, which are designated by Figures W1 and W2 and Movie W1 and are available online at www.neoplasia.com.

[3]These authors equally contributed to this study.

Received 6 March 2012; Revised 10 May 2012; Accepted 14 May 2012

DOI 10.1596/neo.12480

activation of alternate signaling pathways, or molecular heterogeneity within the recurrent tumor. To better understand the mechanisms contributing to drug resistance and the efficacy of combining targeted agents, preclinical evaluation of investigational agents in mouse models of EOC should be informative. We developed a transgenic mouse model of spontaneous EOC by expressing the early region of SV40 under transcriptional control of the Müllerian-inhibiting substance type II receptor [2]. Expression of SV40 TAg genes leads to functional inactivation of p53, Rb, and Rb-related proteins and activation of the AKT/mTOR pathway through inactivation of PP2A [3]. Results from The Cancer Genome Atlas Research Network demonstrated that these are the most common alterations that occur in high-grade serous ovarian carcinoma in women [4]. Female Tg*MISIIR-TAg* transgenic mice develop bilateral ovarian carcinomas with 100% penetrance, and tumors are histologically similar to serous adenocarcinomas in women [5–7]. To facilitate studies of ovarian cancer disease progression and response to therapy, we developed magnetic resonance imaging (MRI) methods for longitudinal *in vivo* anatomic tumor imaging and quantification [5]. Using MRI, we showed that ovarian cancers in Tg*MISIIR-TAg* mice respond to standard combination chemotherapy consisting of cisplatin and paclitaxel [5] and to the mTOR-targeted agent RAD001 (everolimus) [8]. Because tumor growth rate and response to therapy can be quantified, noninvasive longitudinal imaging modalities such as MRI offer considerable advantages over end point assessments for preclinical studies evaluating therapeutic efficacy.

Over the past decade, significant advances have been made in the development and application of *in vivo* molecular imaging in mice [9]. Molecular imaging technology uses fluorescent imaging probes in conjunction with either fluorescence reflectance imaging (FRI) or three-dimensional (3D) fluorescence molecular tomography (FMT) [9]. Target-specific and enzyme activatable fluorescent probes enable detection of molecules or biologic activities of tumors and/or the tumor microenvironment in real time. Importantly, fluorescent probe activation and retention can be quantified using FMT. Although sensitive and quantitative, FMT provides somewhat limited anatomic information and spatial resolution. To overcome this limitation, FMT is often coupled with an imaging modality that provides good spatial and anatomic resolution, such as computed tomography or MRI [10–12]. To date, most tumor models evaluated by FMT are those that are engrafted subcutaneously or that occur spontaneously close to the body surface (e.g., mammary cancer models) [13,14]. *In vivo* FMT imaging of tumors in deeply embedded organs is significantly more challenging than superficial tumors and has not been reported for mouse models of ovarian cancer [10,11].

The goals of this study were to 1) develop and validate methods for *in vivo* fluorescent molecular imaging of spontaneous ovarian tumor development in a transgenic mouse model of EOC, 2) develop multimodal imaging strategies using MRI and FMT for fusion of anatomic and molecular images of ovarian tumors in mice, and 3) determine the correlation of fluorescent optical imaging probe signals with ovarian tumor volume, progression, and response to therapy. Here we describe a dual MRI-FMT imaging approach for detection and quantification of tumor-associated cathepsin protease and matrix metalloproteinase (MMP) activities and integrin $\alpha_v\beta_3$ expression in ovarian carcinomas in living mice with fluorescent molecular imaging probes. This molecular imaging strategy can be used to detect tumor progression and response to therapy *in vivo*.

Materials and Methods

Transgenic Mice

Procedures were approved by the Fox Chase Cancer Center Institutional Animal Care and Use Committee, and mice were maintained under specific pathogen-free conditions. Tg*MISIIR-TAg* mice have been described [2,5] and were genotyped by polymerase chain reaction amplification of the TAg transgene. Mice were maintained on a standard diet (2018SX Teklad Global; Harlan Laboratories, Somerville, NJ) and transitioned to a purified, alfalfa-free rodent chow (Teklad AIN-76A; Harlan Laboratories) for a minimum of 24 hours before fluorescent imaging to minimize fluorescence in the gut.

Cells and Culture Conditions

Murine ovarian carcinoma (MOVCAR) 5009 cells isolated from the ascites of ovarian tumor-bearing Tg*MISIIR-TAg* mice [2,7] were maintained in Dulbecco modified Eagle medium containing 4% fetal bovine serum, penicillin/streptomycin (100 U/ml and 100 μg/ml, respectively), and 1× insulin/transferrin/selenium (supplied as a 100× stock by Life Technologies, Grand Island, NY). Cathepsin protease activity was evaluated using commercially available assay kits for detection of cathepsins B, D, and L (ab65300, ab65302, and ab65306; Abcam, Cambridge, MA). Briefly, 1×10^6 MOVCAR 5009 cells were plated and grown at 37°C for 24 hours, lysed, and assayed according to the manufacturer's instructions.

Optical Imaging Agents

For optical imaging of ovarian tumors and cells, commercially available imaging probes designed to detect oncologic processes were used. Tumor-associated cathepsin and MMP activities were detected with ProSense or MMPSense, respectively, and tumor-associated integrin receptor expression was detected with the integrin $\alpha_v\beta_3$–targeted probe IntegriSense [15]. AnnexinVivo 750, which detects exposed phosphatidyl serine, was used for anatomic localization based on its retention in the kidneys. All probes were purchased from PerkinElmer, Inc (Waltham, MA), and were administered intravenously into anesthetized mice by retro-orbital injection at a dose of 2.0 nmol for *in vivo* experiments.

In Vitro *Detection of Optical Imaging Probes*

Parallel cultures of MOVCAR 5009 cells were grown in the presence and absence of cathepsin protease inhibitors (cathepsin B inhibitor III [CA-074] or cathepsin L inhibitor [CAA0225]; EMD Chemicals, Inc, Gibbstown, NJ) and MMP inhibitors (ARP-100; Tocris Bioscience, Bristol, United Kingdom). For detection of both ProSense 680 and MMPSense 680, 3×10^4 cells were seeded on fibronectin-coated coverslips in 24-well plates for 4 hours and treated with 1 μg/ml saponin to facilitate binding and detection of hydrophobic probes. The medium was replaced with fresh medium containing vehicle (0.2% dimethyl sulfoxide), cathepsin inhibitor (20 μM CA-074 or 20 μM CAA0225) or MMP inhibitor (1 μM of ARP-100). After incubating for 1 hour in the presence or absence of protease inhibitors, 1 nmol/ml of ProSense 680 or MMPSense 680 was added, and cells were incubated for an additional 18 hours. For integrin $\alpha_v\beta_3$ detection, parallel cultures of 3×10^4 cells were grown overnight and treated with 1 μg/ml saponin for 15 minutes. Cells were then incubated in the presence of 0.2% dimethyl sulfoxide or 100 nM echistatin, an integrin $\alpha_v\beta_3$ antagonist (Tocris Bioscience) for 15 minutes, and then the medium was replaced with fresh medium containing 1 nmol/ml IntegriSense 680 and cells were incubated for an additional 15 minutes. Coverslips were washed with phosphate-buffered saline, fixed in 3% paraformaldehyde,

counterstained with DAPI, and probe activation or binding was detected by fluorescence microscopy.

Fluorescence Molecular Tomography

Before imaging, mice were anesthetized with isoflurane (Isosol; Vedco, Inc, St Joseph, MO) at a concentration of 2% in medical-grade O_2, and fur around the lower thorax, the abdomen, and the back was removed by shaving and depilation with a cosmetic hair removal lotion. FMT was performed with the VisEn FMT2500 Quantitative Tomography Imaging *In Vivo* Imaging System (PerkinElmer, Inc). Mice were placed in a biplanar imaging cassette supplied with the instrument and transilluminated with laser light. Resulting transmission and fluorescence patterns were captured with a thermoelectrically cooled CCD camera, and the position and intensity of fluorescence sources were reconstructed in three dimensions using the TrueQuant software package (Perkin Elmer), supplied with the FMT2500 [16]. For ProSense 680, IntegriSense 680, or MMPSense 680, mice were injected with probes and imaged 24 hours later. MMPSense 750 was injected 14 hours before imaging, and AnnexinVivo 750 was injected 2 hours before imaging. All mice were imaged in the both the 680- and 750-nm channels and imaging times totaled approximately 15 minutes for each mouse.

Magnetic Resonance Imaging

MRI was performed in a vertical-bore 7-T magnet with a Bruker DRX300 spectrometer (Bruker Biospin Corporation, Billerica, MA) and ParaVision 3.0 software (Bruker Biospin Corporation) as described [5,17]. A custom-built transfer cassette constructed of a Lucite frame and 0.12-mm-thick mylar windows was used. Both the FMT and MRI cassettes compressed the mice to an equal thickness of 15.0 mm. To ensure accurate image fusion, mice were positioned in precisely the same orientation when transferred from one cassette to another, aligning the inferior-superior axis parallel to the edges of the cassette. Contrast-enhanced MRI was performed as described [5]. Alternatively, mice were imaged using a T2-weighted fast spin echo (rapid acquisition with refocused echoes), which could be completed quickly (~2 min 35 sec) and did not require gadolinium contrast enhancement (T_R = 2400 milliseconds, T_E = 8.8 milliseconds, rapid acquisition with refocused echoes factor = 8, effective echo time = 37 milliseconds, slice thickness = 0.75 mm, field of view = 2.56 cm, in-plane resolution = 0.1 mm, and signal average = 2). Image data sets were converted to Analyze image format and tumor volumes calculated using MRIcro [18] (http://www.cabiatl.com/mricro/) as described [5].

A full-body-thickness MR data set for rendering with FMT was generated using a 3D gradient echo with T_R = 200 milliseconds, T_E = 2.3 milliseconds, flip angle = 60 degrees, and number of excitations = 1 imaging sequence. The acquisition matrix of 256 × 192 × 96 was zero-filled and reconstructed to a matrix of 256 × 256 × 128. The field of view was 3 × 3 × 1.5 cm for an isotropic voxel size of 0.13 mm.

Image Fusion

FMT and MRI data sets were fused using freely available A Medical Imaging Data Examiner (AMIDE) software [19] (http://amide.sourceforge.net/). TrueQuant software permitted exportation of the FMT data sets in DICOM format, whereas the MRI data sets were imported directly into AMIDE, with the relevant scan geometry information entered manually. Image fusion of the two data sets was done using the kidneys as internal fiducial markers. The kidneys were marked and detected in the FMT data set by kidney-specific binding of AnnexinVivo 750 probe, and the data sets were aligned and rotated until the kidneys overlapped in three dimensions. The same transformations that aligned the kidneys in the two data sets were then applied to the FMT data set from the 680-nm channel. The position of the ovaries (or ovarian tumors) relative to the kidneys in the MR data set was noted, and the areas corresponding to ovary were then identified on the FMT data sets as displayed in the TrueQuant software and regions of interest (ROIs) were drawn. The ROIs drawn were of similar volume to those calculated directly from the MR data set. The absolute value of probe retention in the ROI was measured in picomoles (calculated by TrueQuant).

Ex Vivo *FRI*

After *in vivo* imaging, mice were euthanized, dissected to expose the abdominal cavity, and imaged in an IVIS Spectrum (Caliper Life Science, Hopkinton, MA) fluorescent/bioluminescent imaging system. Fluorescent images were acquired with 0.5-second exposure times at *f*-stop = 2. The 680-nm probes were imaged with an excitation wavelength of 640 nm and emission of 700 nm, and the 750-nm probes were imaged with an excitation wavelength of 710 nm and emission at 760 nm. After imaging of the abdomen, mice were further dissected, and excised organs, including the ovaries, the reproductive tract, the kidneys, the intestine, the liver, the spleen, and the lungs, were imaged with the same parameters. ROIs were drawn around each ovarian tumor, and the total radiant efficiency ([p/s]/[μW/cm^2]), as calculated by the Living Image software (supplied with IVIS Spectrum), was recorded.

Chemotherapy

To detect response to chemotherapy with fluorescent probes and FMT, mice were first imaged with MRI to confirm the presence and volume of ovarian tumors. Normal ovaries are approximately 10 mm^3; therefore, the minimum size threshold for initiation of chemotherapy was defined as 25 mm^3. Mice were treated with a standard combination chemotherapy consisting of cisplatin (6 mg/kg, injected intraperitoneally four times at 4-day intervals) and paclitaxel (10 mg/kg, injected intraperitoneally six times at 2-day intervals) or vehicle (phosphate-buffered saline).

Tissue Preparation and Immunohistochemistry

Mice were euthanized by CO_2 asphyxiation and examined by necropsy. Tumor length (l) and width (w) was measured with calipers and volume calculated ($l \times w^2 \times 0.5$). Entire reproductive tracts were removed, fixed in 10% (vol/vol) neutral buffered formalin overnight, and submitted for processing. Ovarian tumors were confirmed by evaluation of tissue sections stained with hematoxylin and eosin (H&E) and antibodies recognizing the SV40 TAg (pAB101, 1:100; Santa Cruz Biotechnology, Santa Cruz, CA) as described [2].

Statistical Analysis

Linear regression analyses were used for comparisons of tumor volume and probe retention. Correlations (R^2 values) for each comparison were calculated, and statistical analyses were performed using a two-tailed unpaired Student's t test. $P \leq .05$ was considered significant. Comparisons of tumors in chemotherapy-treated and vehicle-treated mice were based on four summary observations per group and done using the one-sided Wilcoxon two-sample test.

Results

Fluorescent Probe Activation and/or Binding in MOVCAR Cells

To develop methods for detecting ovarian tumors by FMT, fluorescent molecular probes recognizing tumor-associated molecules or biologic activities were required. Among the available imaging agents were probes selectively activated by cathepsin proteases and MMPs and probes that bind to the tumor-associated integrin $\alpha_v\beta_3$. Human ovarian carcinomas commonly exhibit increased activity and/or expression of cathepsin [20–22], MMPs [23,24], and integrin $\alpha_v\beta_3$ [25–27]; thus, these three classes of probes were logical candidates for FMT detection ovarian tumors. Before the *in vivo* experiments, we evaluated *in vitro* activation and/or binding of each probe in MOVCAR 5009 cells [2,7]. The extent and subtype of cathepsin expression in ovarian tumors and tumor-derived cell lines were unknown; therefore, the expression of cathepsins B, D, and L was evaluated using commercially available assays. Low-level cathepsin B activity was detected in MOVCAR cells but was not inhibited by the cathepsin B–specific inhibitor CA-074, suggesting that it was nonspecific (Figure 1*A*). Little or no cathepsin D activity was detected and was not lysate concentration dependent (Figure 1*A*). Concentration-dependent cathepsin L activity was detected, and this activity was significantly inhibited by the cathepsin L-specific inhibitor CAA0225 (Figure 1*A*), suggesting that it is the predominant cathepsin activated in tumor cells. ProSense is an optically silent imaging probe that becomes strongly fluorescent on cleavage by cancer-associated cathepsins, including cathepsin L. MOVCAR cells incubated in the presence of ProSense exhibited a strong fluorescent signal that was significantly inhibited by the addition of CAA0225 but unaffected by CA-074 (Figure 1*B*). These results are consistent with the enzyme assays and show that ovarian tumor cells express cathepsin protease activity necessary for ProSense probe cleavage and activation.

Cell lines and primary ovarian tumors from Tg*MISIIR-TAg* mice express MMP-2 and MMP-9 (F. Xiao and D. Connolly, unpublished data). Consistent with this, MOVCAR cells incubated in the presence of MMPSense (an MMP-activatable probe) exhibited a strong fluorescent signal that was significantly decreased in the presence of the MMP inhibitor ARP-100 (Figure 1*C*). The integrin $\alpha_v\beta_3$–targeted probe, IntegriSense, also bound to MOVCAR cells, and preincubation with the integrin $\alpha_v\beta_3$ antagonist echistatin significantly inhibited this binding (Figure 1*D*). Taken together, these data show that like human EOCs, tumor cells derived from Tg*MISIIR-TAg* mice express tumor-associated cathepsins, MMPs, and integrin $\alpha_v\beta_3$ and that fluorescent probes targeting these proteins would be useful for *in vivo* optical imaging.

Dual MRI and FMT Imaging and Image Alignment

FMT has been used successfully to image subcutaneous and superficial tumors in mice [28,29], but imaging tumors in deeply embedded abdominal organs is significantly more challenging owing to limited tissue penetration and light scattering. An additional technical challenge is the presence of dark fur and pigmentation in mouse strains commonly used to develop genetically engineered mouse models of cancer. Data regarding the feasibility of optical imaging of abdominal organs using FMT in black mice are limited; therefore, we first evaluated ProSense probe activity in wild-type C57BL/6 mice. Resulting images showed background probe signal in the abdominal cavity including the gastrointestinal tract and liver (Figure W1*A*). To provide additional anatomic data for definitive identification of probe signal emanating specifically from ovaries and ovarian tumors, we sought to combine anatomic imaging by MRI with optical imaging by FMT.

Mice are placed horizontally in the FMT2500 imaging system and vertically (head up) in the MRI system; therefore, potential positional shifts of organs due to gravity needed to be addressed for subsequent alignment of MR and FMT images. Software on the imaging systems did not provide for definition of the skin surface to aid in alignment. However, the data as reconstructed are intrinsically volumetric and could be registered directly with a minimum of processing. The planar surfaces of the imaging cassettes were the most clearly defined surfaces and served as boundaries in both data sets as the first step in image fusion. To further ensure correct alignment, we capitalized on the observation that AnnexinVivo 750 is specifically retained in the kidneys of injected mice, resulting in nonoverlapping signals adjacent to normal ovaries or ovarian tumors (Figure W1, *A* and *B*). Based on the adjacent posterior anatomic location of the ovaries with respect to the kidneys, fluorescently marked kidneys could be effectively used as an internal fiducial for alignment of the MR and FMT images.

Fluorescent images exported from the TrueQuant software in DICOM (Figure W1*A*, *subpanels a-c*) were imported into AMIDE (Figure W1*A*, *subpanels d-f*) and aligned with MR images from the same mouse using the fluorescent signal from the kidneys (Figure W2, *A-C*). In the aligned images from wild-type mice, ProSense probe activation was undetectable in either ovary (Figure W2). The normal histology and structure of the ovaries was confirmed by analyzing H&E- and TAg-stained tissue sections (not shown).

In Vivo *Detection of Cathepsin Activity in Ovarian Tumors*

With established methods for MR and FMT image alignment, *in vivo* detection of cathepsin activity in ovarian tumors was first tested in mice with tumors of similar total volume as determined by MRI (Figure W2). Mice were given intravenous injections of ProSense 680 or ProSense 680 control (a nonactivatable analog) and AnnexinVivo 750 and imaged sequentially by MRI and FMT. Data sets were aligned and showed dorsal fluorescent signals that coaligned with the ovarian tumors in the ProSense 680–injected mouse (Figure W2). The specificity of probe activation was confirmed in the ProSense 680 Control probe–injected mice, where there was no detectable signal at the position of the ovarian tumors (Figure W2). Having confirmed that we could detect cathepsin protease activity in ovarian tumors, we then evaluated a larger cohort of mice including three wild-type C57BL/6 mice and 15 Tg*MISIIR-TAg* mice ranging in age from 107 to 192 days (mean age = 143 days). Aligned data sets (Figure 2, *A-C*) were used to determine the position of the ovaries and assign ROIs for signal quantification (Figure 2*D*). Negligible probe activation was observed in wild-type C57BL/6 mice (Figure W2 and data not shown) but was consistently observed in the ovaries of Tg*MISIIR-TAg* mice. In mice with normal-sized or minimally enlarged ovaries (e.g., mouse 9374; Figure 2*A*), discrete fluorescent signals were detected at the position of the ovary (Figure 2, *B-D*). *Ex vivo* fluorescent images of the exposed abdominal cavity and dissected organs (Figure 2, *E-H*) confirmed the presence of fluorescent signals from AnnexinVivo in the kidneys (Figure 2, *E* and *F*) and ProSense in the ovaries (Figure 2, *G* and *H*). Although the ovaries from this mouse exhibited little or no enlargement, H&E and TAg staining of tissue sections clearly showed the presence of bilateral microscopic (~200-600 μm in diameter) ovarian tumors (Figure 2, *I-L*). In mice with large tumors, prominent

ProSense signals were detected (Figure 3) and *ex vivo* images confirmed the ROIs assigned in the FMT image correctly identified fluorescent signals from the kidneys and the massively enlarged (~900 mm^3) left ovarian tumor (Figure 3, *E* and *F*). H&E and TAg stained sections also confirmed the presence of a large tumor in the left ovary (Figure 3, *I* and *J*) and TAg-positive tumor cells in the right ovary (Figure 3, *K* and *L*). Reconstruction and image rendering of 3D fused MR and FMT images showed bilateral ovarian tumors in a Tg*MISIIR-TAg* mouse (Movie W1). This movie illustrates the dorsal position and extent of the ovarian tumor-specific fluorescent signal in the context of the whole animal and the close posterior location of the ovarian tumors relative to the kidneys. Collectively, these data demonstrate that ovarian tumors express cathepsin activity leading to probe activation and retention. Importantly, tumor-associated cathepsin activity can be

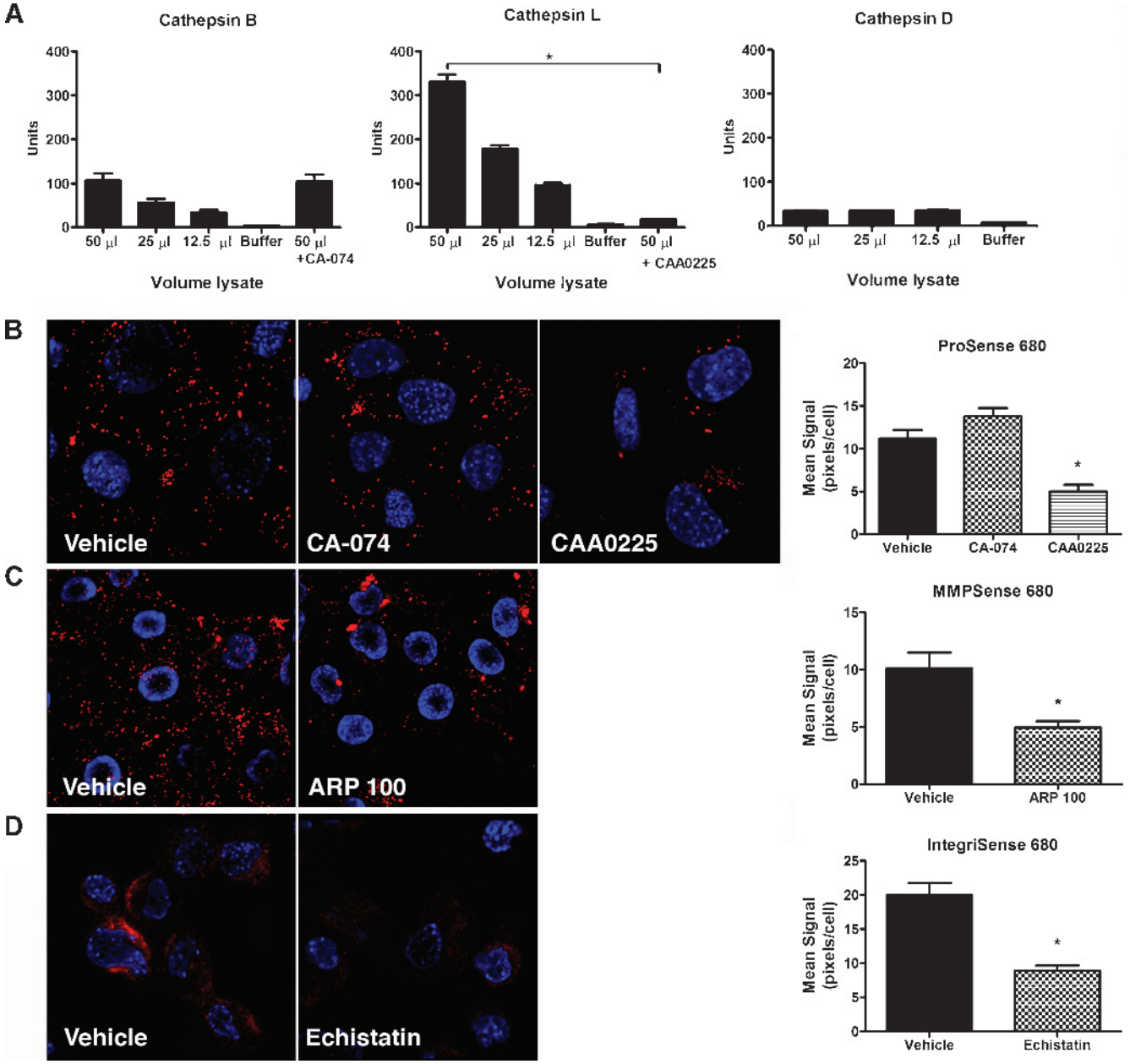

Figure 1. Targeted molecular fluorescent probes detect tumor-associated cathepsin, MMP and integrin $\alpha_v\beta_3$ in MOVCAR cells isolated from tumor-bearing transgenic mice. (A) Lysates of MOVCAR cells assayed for cathepsin activity showed little or no cathepsin B and D activity but exhibited cathepsin L activity that was significantly inhibited by the addition of CAA0225. Mean values and SEM are shown for three independent assays. Cathepsin L activity in untreated and CAA0225-treated cells was compared with unpaired *t* test. *$P < .0001$. (B) MOVCAR cells incubated in the presence of ProSense 680 exhibit probe activation that is inhibited by the cathepsin L–specific inhibitor, CAA0225, but not by the cathepsin B inhibitor CA-074. (C) MOVCAR cells incubated in the presence of MMPSense 680 exhibit probe activation that was significantly inhibited by the addition of the MMP inhibitor ARP-100. (D) Integrin $\alpha_v\beta_3$ probe binding was detected by incubating MOVCAR cells in the absence and presence of the integrin $\alpha_v\beta_3$ antagonist echistatin. Probe activation and retention were quantified by calculating the mean fluorescent signal intensity in 10 cells per field in three image fields using ImageJ and analyzed by analysis of variance, followed by the Tukey multiple comparison test (B, *$P < .001$) or by the unpaired *t* test (C and D, *$P \leq .001$).

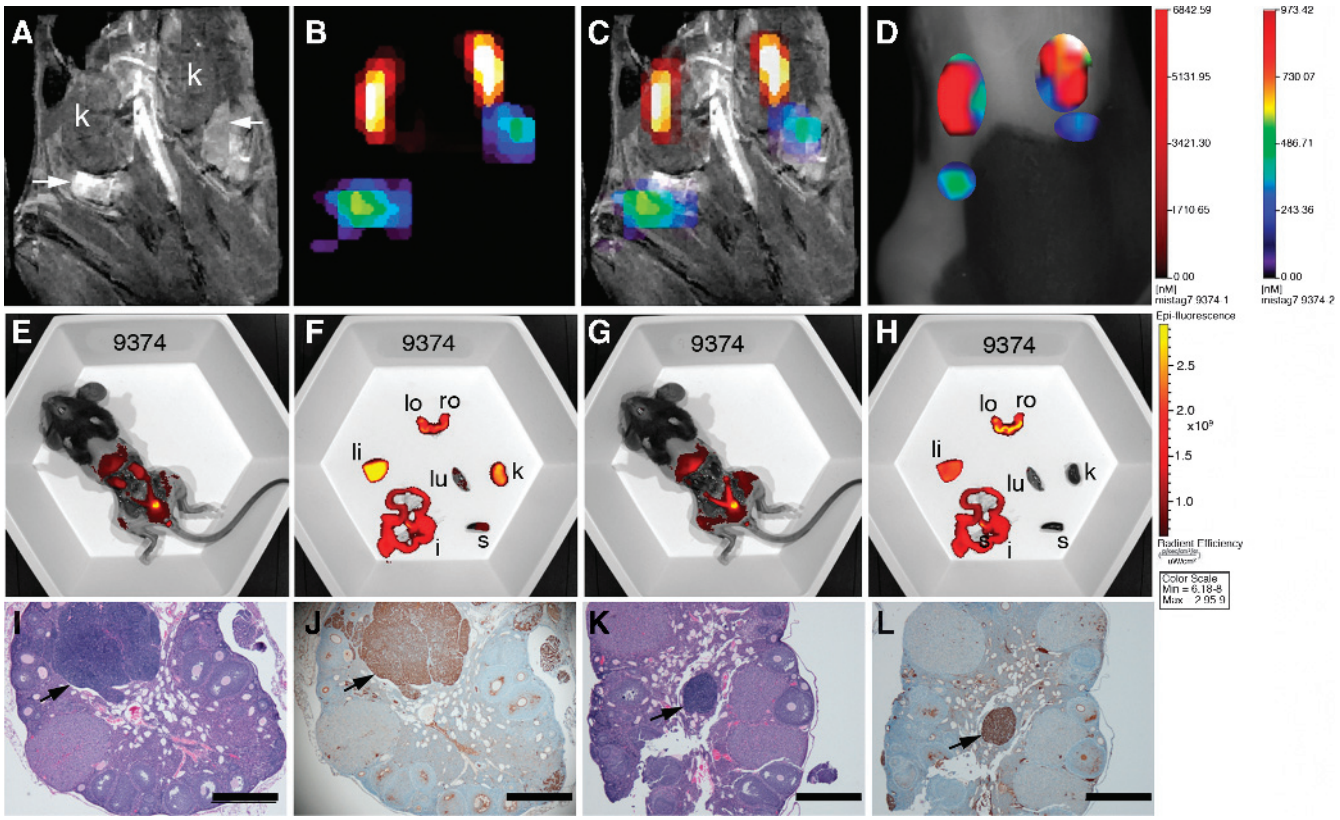

Figure 2. Detection of cathepsin activity in Tg*MISIIR-TAg* mouse with small ovarian tumors. (A) MR image showing essentially normal-sized ovaries (arrows) posterior to the kidneys (k). All MR and fluorescent images in this and in subsequent figures are shown from the dorsal perspective, where the left side of the mouse is on the left side of the image. (B) Fused FMT-MR image showing AnnexinVivo 750 detection of kidneys (yellow-orange and ProSense 680 detection of ovarian tumors (green/blue). (C) Overlay of FMT signals on the MR image. (D) TrueQuant image of the same mouse showing ROIs corresponding to kidney (red) and ovarian tumors (green/blue). Mice were imaged *ex vivo* (E-H) using the IVIS imaging system. Images in E and F were taken with 710-nm excitation and 760-nm emission filters, and those in G and H were taken with 640-nm excitation and 700-nm emission filters. After euthanasia, mice were partially dissected to expose the intact reproductive tract and kidneys (E and G). The reproductive tracts, left ovary (lo), right ovary (ro), and other organs, including liver (li), lung (lu), intestines (i), spleen (s), and kidney (k), were removed and imaged *ex vivo* using the 710/760 and 640/700 filter pairs (F and H, respectively). H&E- (I and K) and TAg- (J and L) stained sections show the presence of microscopic ovarian tumors (arrows) that exhibit strong nuclear TAg staining. Scale bars in H&E- and TAg-stained sections correspond to 500 μm.

detected at an early stage in microscopic ovarian tumors before ovarian enlargement detectable by MRI.

Cathepsin-Mediated Probe Activation Correlates with Tumor Size

Although the spatial resolution of FMT compares poorly with that achievable by MRI for tumor volume quantification, the increased fluorescent signal in mice with large tumors did suggest the possibility that cathepsin activity correlated with tumor size. As this was a first effort at *in vivo* fluorescent molecular imaging of ovarian tumors, direct determination of the probe distribution and the relationship to tumor volume is important to validate the use of fluorescent probes in this model. To evaluate this further, the following comparisons were made for ovarian tumors: 1) volume determined by MRI and caliper measurements, 2) fluorescent probe retention and MRI volume, 3) fluorescent probe retention and caliper volume, 4) *ex vivo* fluorescence reflectance and MRI volume, 5) *ex vivo* fluorescence reflectance and caliper volume, and 6) fluorescent probe retention and *ex vivo* fluorescence reflectance (Figure 4 and Table 1; data not shown). As shown previously [5], an extremely strong correlation existed between tumor volumes determined by MRI and caliper measurement (Figure 4*A*; R^2 = 0.99, P < .0000001). Similarly, cathepsin-mediated probe activation and retention in the ovary were highly correlated with tumor volume determined by MRI (Figure 4*B*; R^2 = 0.95, P < .00001) or by caliper measurement (Figure 4*C*; R^2 = 0.96, P < .0000001). Signal detected by *ex vivo* fluorescence reflectance also correlated with tumor volume (R^2 = 0.69 for MRI and R^2 = 0.73 for calipers, P < .0000001) and probe retention (R^2 = 0.80, P < .0000001; data not shown). Taken together, these results demonstrate that ProSense can be used to detect ovarian tumors in Tg*MISIIR-TAg* mice and that the level of cathepsin activity present in the tumors is strongly correlated with tumor size.

In Vivo *Detection of $\alpha_v\beta_3$ Integrin Binding and MMP Activity in Ovarian Tumors*

Expression of integrin $\alpha_v\beta_3$ has been shown in human ovarian carcinoma cell lines and is associated with motility and invasion mediated by MMPs [25–27]. Based on the *in vitro* data confirming the detection of integrin $\alpha_v\beta_3$ binding and MMP activity in MOVCAR cells (Figure 1), we evaluated IntegriSense and MMPSense for detection of

ovarian tumors *in vivo*. Tg*MISIIR-TAg* (n = 5) and wild-type (n = 2) mice were injected with IntegriSense 680 and AnnexinVivo 750 and imaged by MRI and FMT as described. Strong fluorescent signals were detected in the ovarian tumors of all five of the Tg*MISIIR-TAg* mice (Figure 5, *A-C*) but not in the ovaries of wild-type C57BL/6 mice (not shown). The presence of ovarian tumors was confirmed by histopathologic evaluation of H&E- and TAg-stained sections (not shown). Comparisons of probe retention and tumor volume showed that the IntegriSense signal was strongly correlated with volume determined by MRI (R^2 = 0.93, P < .00001) or caliper measurement (R^2 = 0.88, P < .0001). These results demonstrate that integrin $\alpha_v\beta_3$ expression can be detected in ovarian tumors *in vivo* using IntegriSense and that probe binding correlates with tumor size.

MMP activity in ovarian tumors was evaluated with MMPSense and was detected in ovarian tumors (Figure 5, *D-F*) but not in normal ovaries in wild-type mice (not shown). The presence of ovarian tumors was confirmed by both *ex vivo* imaging and evaluation of H&E- and TAg-stained sections for each case (not shown). The total amount of MMP-mediated probe activation in ovarian tumors was generally lower than the amount of cathepsin or integrin $\alpha_v\beta_3$ probe signal in similar-sized tumors and comparisons of probe retention with tumor volume showed that the absolute amount of MMPSense detected in tumors correlated less well with tumor volume (R^2 = 0.546 for MRI and 0.5997 for calipers, P < .01; data not shown).

Detection of Tumor Progression and Response to Chemotherapy by FMT

Primary ovarian tumors in Tg*MISIIR-TAg* mice have a mean doubling time of 7.3 days and are responsive to standard combination chemotherapy consisting of cisplatin and paclitaxel [5]. Using detection integrin $\alpha_v\beta_3$ probe binding as a surrogate for tumor size, we next tested whether FMT could reliably detect tumor progression and response to chemotherapy in Tg*MISIIR-TAg* mice. Tumor-bearing mice (n = 8) underwent MRI and FMT to determine baseline tumor volume and IntegriSense retention. Mice (n = 4 per group) were then treated with cisplatin and paclitaxel or vehicle and serially imaged by MRI and FMT at 12-day intervals. Ovarian tumors in untreated mice progressed rapidly, exhibiting a tumor doubling time of approximately 1 week (Figure 6, *A* and *C*). The increase in tumor growth was also reflected in a parallel increase in IntegriSense probe binding (Figure 6*D*). Mice treated with cisplatin and paclitaxel exhibited a reduction in ovarian tumor volume detected by MRI (Figure 6, *B* and *C*) and

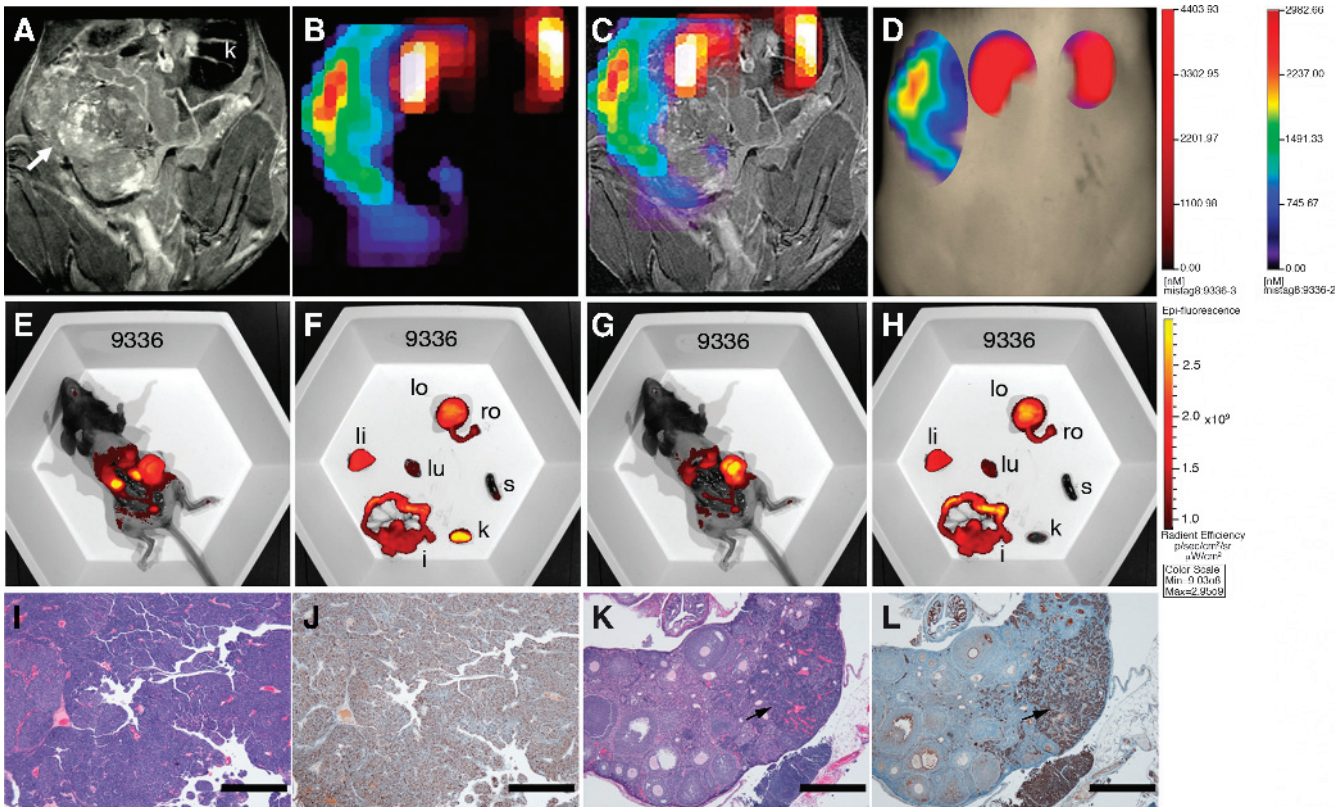

Figure 3. Detection of cathepsin activity in Tg*MISIIR-TAg* mouse with a large ovarian tumor. (A) MR image showing a large ovarian tumor on the left (arrow) and the right kidney (k). (B) AMIDE image showing AnnexinVivo 750 detection of kidneys (yellow-orange) and ProSense 680 detection of the ovarian tumor on the left (red/yellow/green/blue). (C) Overlay of FMT signals on the MR image. (D) TrueQuant image of the same mouse showing ROIs corresponding to kidneys (red) and ovarian tumor on the left (red/yellow/green/blue). Mice were imaged *ex vivo* (E-H) using the IVIS imaging system. Images were taken with either a 710/760-nm filter set (E and F) or a 640/700-nm filter set (G and H). After euthanasia, mice were partially dissected to expose the intact reproductive tract and kidneys (E and G). The reproductive tracts, left ovary (lo), right ovary (ro), and other organs, including liver (li), lung (lu), intestines (i), spleen (s), and kidney (k), were removed and imaged *ex vivo* (F and H) using the 710 and 640 channels, respectively. H&E- (I and K) and TAg- (J and L) stained sections show the presence of a large ovarian tumor on the left and TAg-positive tumor cells within the otherwise normal-sized right ovary (arrows) and outside the ovary within the intrabursal space (arrowheads). Scale bars in H&E- and TAg-stained sections correspond to 500 μm.

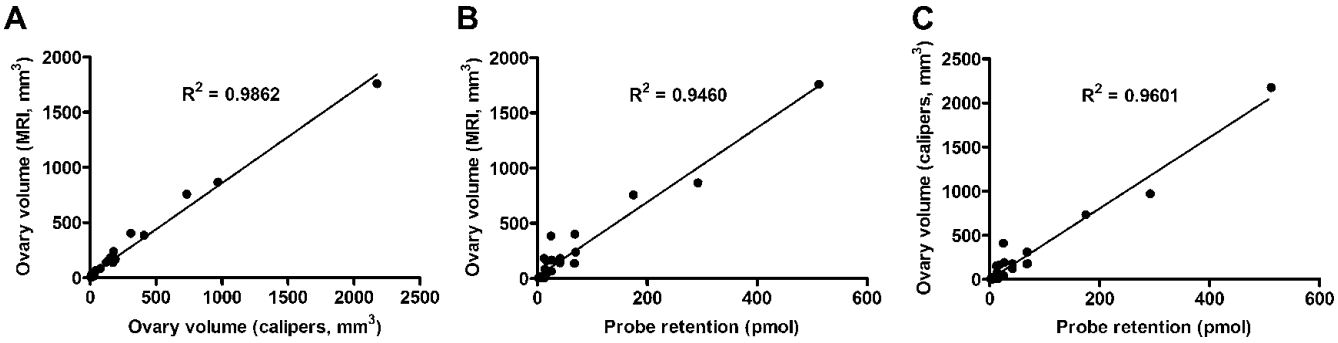

Figure 4. Relationship between cathepsin-mediated ProSense 680 activation and tumor volume. Linear regression analysis of ovarian tumor volume determined by MRI or caliper measurements and cathepsin-mediated activation of the NIRF imaging probe ProSense 680 in tumors. Data from *in vivo* imaging by MRI and FMT were analyzed to compare (A) tumor volume determined by MRI *versus* caliper measurements, (B) probe retention *versus* MRI tumor volume, and (C) probe retention *versus* caliper tumor volume.

significantly decreased probe retention in the tumors (Figure 6, *B* and *D*). Probe retention in the ovarian tumors mice remained strongly correlated with tumor volume determined by MRI or caliper measurements (R^2 = 0.92 and R^2 = 0.86, respectively, $P < .001$; data not shown). Together, these data show that ovarian tumor progression and response to combination chemotherapy can be accurately assessed using FMT with an integrin $\alpha_v\beta_3$–binding fluorescent probe.

Discussion

Using a dual MRI-FMT imaging approach, we confirmed the feasibility and sensitivity of detection of tumor-associated biologic activities in ovarian carcinomas in living mice by FMT imaging with fluorescent molecular imaging probes. For this study, we chose probes based on their relevance to EOC. Among these, the ProSense, MMPSense, and IntegriSense probes were considered to be highly relevant based on prior studies showing high levels of expression and activity of cathepsins, MMPs, and integrin $\alpha_v\beta_3$ in human EOCs [20–27,30–35]. Although immunohistochemical staining is commonly used for detection of proteases in tumor tissues, the mere presence of these proteins does not provide information about protease activity. An advantage of activatable fluorescent probes is that the probes are fluorescently quenched until they are cleaved by active proteases. Thus, probe activation and retention in tumors are directly reflective of tumor-associated protease activity. The fluorescent molecular probes used detected cathepsin and MMP activity and integrin $\alpha_v\beta_3$ binding in ovarian tumors but not in

Table 1. Data Summarizing Probe Concentration (ProSense 680) and Ovarian Tumor Volume from Tg*MISIIR-TAg* Mice.

Mouse No.	Age (d)	Tumor Volume (mm^3)					
		Caliper		MRI		Probe Concentration (pmol)	
		Left Ovary	Right Ovary	Left Ovary	Right Ovary	Left Ovary	Right Ovary
ProSense 680							
9374	107	4.0	9.4	5.0	15.3	6.1	4.9
9375	107	4.5	12.6	5.8	9.1	12.3	12.9
9435	118	30.3	178.9	16.8	238.9	9.1	69.4
9336	122	968.8	7.8	866.8	5.6	292.0	5.2
9264	131	14.0	12.5	11.3	10.2	12.8	6.2
9660	132	732.1	5.3	757.3	6.5	174.7	8.6
9181	147	178.5	42.0	182.7	66.8	41.5	25.5
9180	147	24.5	15.3	14.9	8.38	11.0	29.4
9233	147	9.2	12.8	27.8	14.0	15.5	12.4
9319	154	152.1	409.1	181.7	386.2	12.2	24.7
9075	157	8.4	3.2	6.5	6.9	6.5	6.9
9077	157	174.0	22.3	138.0	11.9	67.4	5.9
9230	159	2174.2	122.4	1758.4	142.4	512.3	29.2
9320	174	77.5	191.1	85.7	168.9	13.4	26.3
9265	192	308.4	161.8	402.2	161.0	40.23	17.3
IntegriSense 680							
9603	97	69.8	2258.3	44.8	1358.8	5.5	199.8
9315	125	3.3	10.3	11.8	23.5	0.0	24.9
9245	140	310.0	13.3	206.8	19.6	20.5	24.3
9232	147	487.4	134.6	430.0	141.3	112.3	46.0
9079	157	16	16.8	29.4	13.1	21.6	16.6
MMPSense 680							
9661	139	473.8	1.8	379.7	5.8	19.1	1.0
9516	145	19.5	57.4	17.8	34.7	2.3	10.1
9646	148	793.2	654.2	585.6	803.0	67.1	41.7
9462	155	855.6	87.5	743.9	29.2	20.0	2.2
9698	157	4.0	537.0	14.5	460.2	2.9	12.5

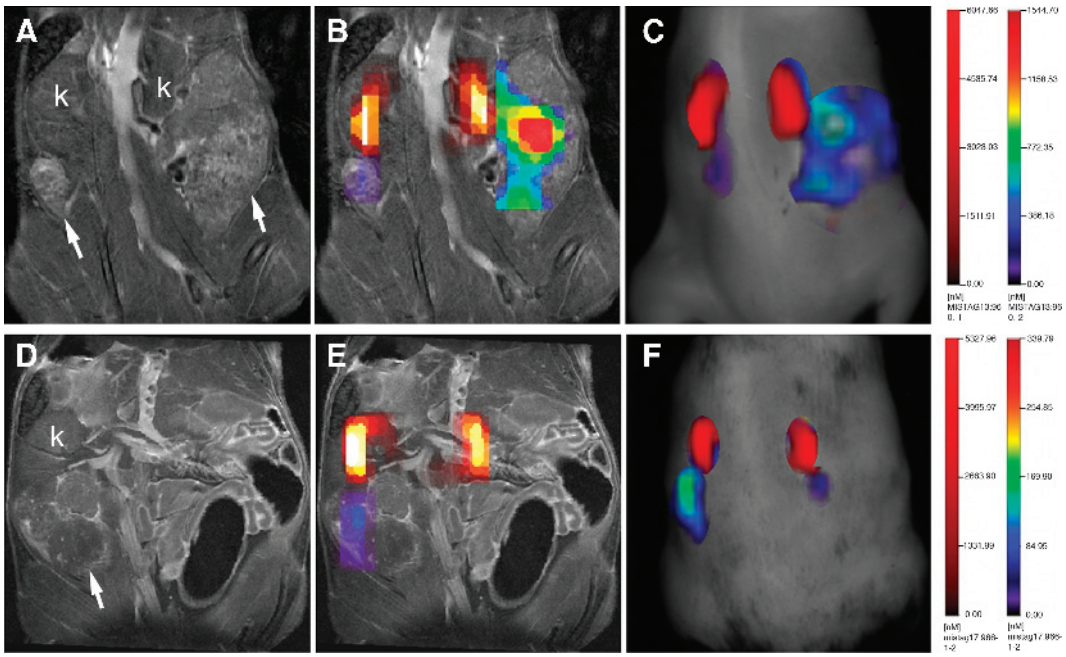

Figure 5. Detection of ovarian tumors with IntegriSense 680 and MMPSense 680 probes. (A) MR image showing bilateral ovarian tumors (arrows), (B) fused FMT-MR image, and (C) TrueQuant images of a mouse injected systemically with IntegriSense 680 and AnnexinVivo 750. (D) MR, (E) fused FMT-MR, and (F) TrueQuant images of a mouse injected systemically with MMPSense 680 and AnnexinVivo 750.

normal wild-type ovaries. Quantitative assessments showed that cathepsin activity and integrin $\alpha_v\beta_3$ binding were strongly correlated with tumor volume. MMP activity was readily detected in ovarian tumors; however, the correlation with tumor volume was not as strong. This may be related to differences in: 1) overall MMP activity in tumors, 2) lack of uniform MMP activity in tumors, or 3) intrinsic differences in the imaging probes properties (e.g., inherent fluorescent signal strength and/or capacity for tumor localization and penetration).

Advances in optical molecular imaging technologies offer the possibility of improved or alternative strategies for disease detection and staging and for the identification and observation of molecules and/or biologic activities associated with tumor initiation, progression and response to therapy. Importantly, in the current study, fluorescent probes targeting tumor-associated protease activity allowed *in vivo* detection of microscopic tumors in mice before enlargement of the ovary detectable by MRI. In addition, FMT coupled with a fluorescent probe detecting integrin $\alpha_v\beta_3$ binding enabled *in vivo* detection of both tumor progression and response to chemotherapy. The $\alpha_v\beta_3$ integrin binding signal detected in ovarian tumors may be from tumor cells, tumor vasculature or both. However, the FMT2500 instrumentation is not sufficiently sensitive to discriminate between these possibilities.

The findings in this study support additional investigation of molecular imaging for *in vivo* early detection of ovarian tumors and for detection of functional response to targeted therapy. Some targeted and immune-based therapeutic agents show efficacy in the absence of radiologic evidence of tumor regression or in some cases after initial evidence of progressive disease [36,37]. Therefore, optical assessments of biologic activities within tumors may provide relevant information regarding response to therapy in the absence of detectable changes in tumor volume achieved by anatomic imaging. Although beyond the scope of the present study, demonstration of value added by FMT-based imaging to the already highly sensitive and reliable anatomic imaging provided by MRI will require additional studies, the success of which will require the identification of a molecular targeted agent with significant antitumor activity for EOC and the availability of fluorescent probes that bind to or are activated by relevant downstream biologic mediators of the pathway targeted.

Until recently, *in vivo* optical imaging strategies primarily relied on planar imaging methods (e.g., fluorescence reflectance or bioluminescent imaging) that, although informative, are nonquantitative and subject to significant limitations of light penetration and scattering in tissues [13]. Improvements in tomographic optical imaging technology and fluorescent imaging probes with high target-to-background ratios and low tissue autofluorescence led to the availability of FMT instrumentation and its application for small animal imaging [38]. Whereas FMT instrumentation theoretically enables imaging of fluorescent signals at depths more than 500 μm, there is little available information regarding *in vivo* fluorescent molecular imaging of ovarian tumors in mice. Previous studies in mice with xenografts of human EOC cells demonstrated the feasibility of optical imaging using fluorescent probes for detection of tumor nodules but largely relied on *ex vivo* FRI [39,40]. The results of this study demonstrate for the first time the feasibility, sensitivity, and accuracy of fluorescent imaging probes and FMT for *in vivo* detection of spontaneous ovarian tumors in black mice and for quantification of tumor-associated biologic activities.

Because FMT was a new approach for *in vivo* imaging of spontaneous ovarian tumors, the combined imaging strategy increased the accuracy of detection and quantification of tumor-specific fluorescent probe activation/retention. The major challenge in image alignment was due to the gravitational effects on the organs in mice imaged in the vertical position for MRI compared with the horizontal position for FMT. Co-administration of AnnexinVivo to mark the kidneys for image alignment helped overcome this challenge. The observation of high AnnexinVivo probe accumulation in the kidneys is consistent with previous reports showing increased apoptosis and accumulation of exposed phosphatidyl serine in the proximal tubules of kidney after isoflurane

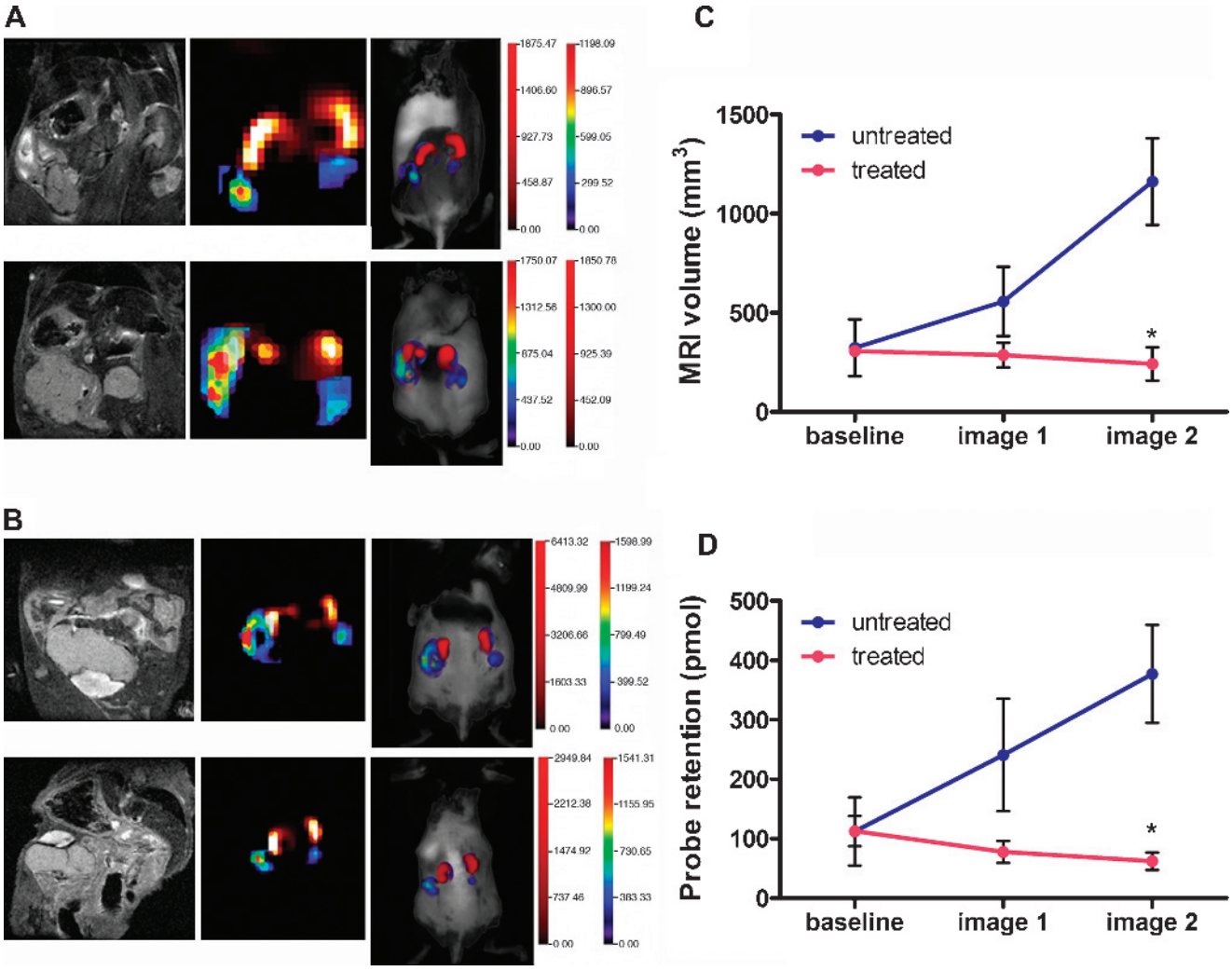

Figure 6. Serial FMT imaging detecting tumor progression and response to chemotherapy. Mice ($n = 8$) were injected with IntegriSense 680 and received baseline FMT and MRI scans 24 hours later. Immediately after the baseline scan, mice were either injected with vehicle ($n = 4$) or were treated with combination chemotherapy ($n = 4$) and subsequently imaged twice at 12-day intervals (image 1 = day 12, image 2 = day 24). Representative images are shown for untreated (A) and chemotherapy-treated (B) mice, with baseline images on top and the second serial image at the bottom. A strong correlation was observed between tumor volume by MRI (C) and probe retention (D). Mean values ± SEM of the treated (red lines) and untreated (blue lines) mice are shown, and the mean differences in tumor size and probe retention in treated and untreated mice were significant ($P < .001$).

inhalation [41] as well as studies using technetium 99m–conjugated annexin V imaging agents showing that these agents are retained in the kidneys of mice and humans [42,43]. Given the proximal location of kidneys to the ovaries, this approach was more effective than external installation of fiducial markers and allowed the use of the same anatomic structure as a fiducial for serial images. The imaging methods described in this work will be easily adaptable to imaging mice with orthotopic implants of human ovarian cancer cells or patient tumor tissue in the intrabursal space [17].

Technical limitations related to the depth of tissue imaging make clinical adaptation of FMT imaging unlikely. However, the development of combination fluorescent and white light endoscopes has allowed *in vivo* imaging of disseminated peritoneal tumor nodules using cathepsin activatable or small-molecule fluorescent imaging probes [44,45]. The use of fluorescent imaging probes with high tumor-to-background ratios results in increased sensitivity and specificity in the detection of tumor nodules compared to white light imaging. Continued advancements in clinical adaptation of endoscopic fluorescent imaging technology and approval of activatable and/or targeted fluorescent probes for clinical use are predicted to improve surgical staging and optimal surgical debulking by detection of small disseminated lesions that are not visible by conventional white light imaging.

The need for alternative therapies for EOC is underscored by the common development of resistance to standard cytotoxic chemotherapy and the persistently high mortality rate associated with advanced stage ovarian cancer [46]. Many targeted molecular therapies are available, several of which have been evaluated in clinical trials; however, there are few examples with demonstrated clinical efficacy for the majority of patients. Given the high degree of tumor heterogeneity [4], EOC treatment may require a more individualized approach. High-throughput genomic and proteomic analyses of individual tumor specimens may identify genes and signaling pathways that contribute to cancer progression, but determining the most effective single agents or combinations remains a significant challenge. Studies in mouse models

have the potential to facilitate the rapid evaluation of novel agents and effective drug combinations. Whereas the standard assessment of response to therapy is tumor regression, disease stabilization may be an acceptable clinical outcome. Multimodal imaging approaches for evaluation of changes in metabolic or biologic activity of the tumor may suggest a positive response to treatment. Further development of fluorescent molecular imaging probes is predicted to result in additional agents that can be used as biomarkers of functional response to a variety of targeted therapies. Importantly, the use of FMT for fluorescent imaging in preclinical models can provide quantitative information regarding specific probe activation and retention as well as response to therapy and is predicted to have translational applications for detection, staging, and treatment of ovarian cancer.

Acknowledgments

The authors thank Margie Clapper, Michael Seiden, Timothy Yen, and Ronald Wolf for helpful discussions and critical review of this article.

References

[1] Jemal A, Siegel R, Xu J, and Ward E (2010). Cancer statistics, 2010. *CA Cancer J Clin* **60**, 277–300.

[2] Connolly DC, Bao R, Nikitin AY, Stephens KC, Poole TW, Hua X, Harris SS, Vanderhyden BC, and Hamilton TC (2003). Female mice chimeric for expression of the simian virus 40 TAg under control of the MISIIR promoter develop epithelial ovarian cancer. *Cancer Res* **63**, 1389–1397.

[3] Cheng J, DeCaprio JA, Fluck MM, and Schaffhausen BS (2009). Cellular transformation by Simian virus 40 and murine polyoma virus T antigens. *Semin Cancer Biol* **19**, 218–228.

[4] Network TCGAR (2011). Integrated genomic analyses of ovarian carcinoma. *Nature* **474**, 609–615.

[5] Kurman RJ and Shih Ie M (2010). The origin and pathogenesis of epithelial ovarian cancer: a proposed unifying theory. *Am J Surg Pathol* **34**, 433–443.

[6] Hensley H, Quinn BA, Wolf RL, Litwin SL, Mabuchi S, Williams SJ, Williams C, Hamilton TC, and Connolly DC (2007). Magnetic resonance imaging for detection and determination of tumor volume in a genetically engineered mouse model of ovarian cancer. *Cancer Biol Ther* **6**, 1717–1725.

[7] Quinn BA, Xiao F, Bickel L, Martin L, Hua X, Klein-Szanto A, and Connolly DC (2010). Development of a syngeneic mouse model of epithelial ovarian cancer. *J Ovarian Res* **3**, 24.

[8] Mabuchi S, Altomare DA, Connolly DC, Klein-Szanto A, Litwin S, Hoelzle MK, Hensley HH, Hamilton TC, and Testa JR (2007). RAD001 (everolimus) delays tumor onset and progression in a transgenic mouse model of ovarian cancer. *Cancer Res* **67**, 2408–2413.

[9] Weissleder R (2006). Molecular imaging in cancer. *Science* **312**, 1168–1171.

[10] Grimm J, Kirsch DG, Windsor SD, Kim CF, Santiago PM, Ntziachristos V, Jacks T, and Weissleder R (2005). Use of gene expression profiling to direct *in vivo* molecular imaging of lung cancer. *Proc Natl Acad Sci USA* **102**, 14404–14409.

[11] Kirsch DG, Dinulescu DM, Miller JB, Grimm J, Santiago PM, Young NP, Nielsen GP, Quade BJ, Chaber CJ, Schultz CP, et al. (2007). A spatially and temporally restricted mouse model of soft tissue sarcoma. *Nat Med* **13**, 992–997.

[12] Weissleder R and Ntziachristos V (2003). Shedding light onto live molecular targets. *Nat Med* **9**, 123–128.

[13] Ntziachristos V, Ripoll J, Wang LV, and Weissleder R (2005). Looking and listening to light: the evolution of whole-body photonic imaging. *Nat Biotechnol* **23**, 313–320.

[14] Zacharakis G, Kambara H, Shih H, Ripoll J, Grimm J, Saeki Y, Weissleder R, and Ntziachristos V (2005). Volumetric tomography of fluorescent proteins through small animals *in vivo*. *Proc Natl Acad Sci USA* **102**, 18252–18257.

[15] Kossodo S, Pickarski M, Lin SA, Gleason A, Gaspar R, Buono C, Ho G, Blusztajn A, Cuneo G, Zhang J, et al. (2009). Dual *in vivo* quantification of integrin-targeted and protease-activated agents in cancer using fluorescence molecular tomography (FMT). *Mol Imaging Biol* **12**, 488–499.

[16] Graves EE, Weissleder R, and Ntziachristos V (2004). Fluorescence molecular imaging of small animal tumor models. *Curr Mol Med* **4**, 419–430.

[17] Connolly DC and Hensley HH (2009). Xenograft and transgenic mouse models of epithelial ovarian cancer and non-invasive imaging modalities to monitor ovarian tumor growth *in situ*: applications in evaluating novel therapeutic agents. *Current Protoc Pharmacol* **45**, 14.12.11–14.12.36.

[18] Rorden C and Brett M (2000). Stereotaxic display of brain lesions. *Behav Neurol* **12**, 191–200.

[19] Loening AM and Gambhir SS (2003). AMIDE: a free software tool for multimodality medical image analysis. *Mol Imaging* **2**, 131–137.

[20] Chai Y, Wu W, Zhou C, and Zhou J (2012). The potential prognostic value of cathepsin D protein in serous ovarian cancer. *Arch Gynecol Obstet*. E-pub ahead of print.

[21] Downs LS Jr, Lima PH, Bliss RL, and Blomquist CH (2005). Cathepsins B and D activity and activity ratios in normal ovaries, benign ovarian neoplasms, and epithelial ovarian cancer. *J Soc Gynecol Investig* **12**, 539–544.

[22] Losch A, Schindl M, Kohlberger P, Lahodny J, Breitenecker G, Horvat R, and Birner P (2004). Cathepsin D in ovarian cancer: prognostic value and correlation with p53 expression and microvessel density. *Gynecol Oncol* **92**, 545–552.

[23] Moser TL, Young TN, Rodriguez GC, Pizzo SV, Bast RC Jr, and Stack MS (1994). Secretion of extracellular matrix–degrading proteinases is increased in epithelial ovarian carcinoma. *Int J Cancer* **56**, 552–559.

[24] Schmalfeldt B, Prechtel D, Harting K, Spathe K, Rutke S, Konik E, Fridman R, Berger U, Schmitt M, Kuhn W, et al. (2001). Increased expression of matrix metalloproteinases (MMP)-2, MMP-9, and the urokinase-type plasminogen activator is associated with progression from benign to advanced ovarian cancer. *Clin Cancer Res* **7**, 2396–2404.

[25] Beck V, Herold H, Benge A, Luber B, Hutzler P, Tschesche H, Kessler H, Schmitt M, Geppert HG, and Reuning U (2005). ADAM15 decreases integrin $\alpha_v\beta_3$/vitronectin–mediated ovarian cancer cell adhesion and motility in an RGD-dependent fashion. *Int J Biochem Cell Biol* **37**, 590–603.

[26] Landen CN, Kim TJ, Lin YG, Merritt WM, Kamat AA, Han LY, Spannuth WA, Nick AM, Jennnings NB, Kinch MS, et al. (2008). Tumor-selective response to antibody-mediated targeting of $\alpha_v\beta_3$ integrin in ovarian cancer. *Neoplasia* **10**, 1259–1267.

[27] Leroy-Dudal J, Demeilliers C, Gallet O, Pauthe E, Dutoit S, Agniel R, Gauduchon P, and Carreiras F (2005). Transmigration of human ovarian adenocarcinoma cells through endothelial extracellular matrix involves α_v integrins and the participation of MMP2. *Int J Cancer* **114**, 531–543.

[28] Bremer C, Ntziachristos V, Weitkamp B, Theilmeier G, Heindel W, and Weissleder R (2005). Optical imaging of spontaneous breast tumors using protease sensing "smart" optical probes. *Invest Radiol* **40**, 321–327.

[29] von Wallbrunn A, Holtke C, Zuhlsdorf M, Heindel W, Schafers M, and Bremer C (2007). *In vivo* imaging of integrin $\alpha_v\beta_3$ expression using fluorescence-mediated tomography. *Eur J Nucl Med Mol Imaging* **34**, 745–754.

[30] Athanassiadou P, Sakellariou V, Petrakakou E, Athanassiades P, Zerva C, Liossi A, and Michalas S (1998). Cathepsin D immunoreactivity in ovarian cancer: correlation with prognostic factors. *Pathol Oncol Res* **4**, 103–107.

[31] Baekelandt M, Holm R, Trope CG, Nesland JM, and Kristensen GB (1999). The significance of metastasis-related factors cathepsin-D and nm23 in advanced ovarian cancer. *Ann Oncol* **10**, 1335–1341.

[32] Fishman DA, Liu Y, Ellerbroek SM, and Stack MS (2001). Lysophosphatidic acid promotes matrix metalloproteinase (MMP) activation and MMP-dependent invasion in ovarian cancer cells. *Cancer Res* **61**, 3194–3199.

[33] Naylor MS, Stamp GW, Davies BD, and Balkwill FR (1994). Expression and activity of MMPS and their regulators in ovarian cancer. *Int J Cancer* **58**, 50–56.

[34] Sakata K, Shigemasa K, Nagai N, and Ohama K (2000). Expression of matrix metalloproteinases (MMP-2, MMP-9, MT1-MMP) and their inhibitors (TIMP-1, TIMP-2) in common epithelial tumors of the ovary. *Int J Oncol* **17**, 673–681.

[35] Scambia G, Panici PB, Ferrandina G, Salerno G, D'Agostino G, Distefano M, de Vincenzo R, Ercoli A, and Mancuso S (1994). Clinical significance of cathepsin D in primary ovarian cancer. *Eur J Cancer* **30A**, 935–940.

[36] Eisenhauer EA, Therasse P, Bogaerts J, Schwartz LH, Sargent D, Ford R, Dancey J, Arbuck S, Gwyther S, Mooney M, et al. (2009). New response evaluation criteria in solid tumours: revised RECIST guideline (version 1.1). *Eur J Cancer* **45**, 228–247.

[37] Wolchok JD, Hoos A, O'Day S, Weber JS, Hamid O, Lebbe C, Maio M, Binder M, Bohnsack O, Nichol G, et al. (2009). Guidelines for the evaluation of immune therapy activity in solid tumors: immune-related response criteria. *Clin Cancer Res* **15**, 7412–7420.

[38] Hilderbrand SA and Weissleder R (2009). Near-infrared fluorescence: application to *in vivo* molecular imaging. *Curr Opin Chem Biol* **14**, 71–79.

[39] Gunn AJ, Hama Y, Koyama Y, Kohn EC, Choyke PL, and Kobayashi H (2007). Targeted optical fluorescence imaging of human ovarian adenocarcinoma using a galactosyl serum albumin-conjugated fluorophore. *Cancer Sci* **98**, 1727–1733.

[40] Hama Y, Urano Y, Koyama Y, Gunn AJ, Choyke PL, and Kobayashi H (2007). A self-quenched galactosamine-serum albumin-rhodamineX conjugate: a "smart" fluorescent molecular imaging probe synthesized with clinically applicable material for detecting peritoneal ovarian cancer metastases. *Clin Cancer Res* **13**, 6335–6343.

[41] Lee HT, Kim M, Kim J, Kim N, and Emala CW (2007). TGF-β1 release by volatile anesthetics mediates protection against renal proximal tubule cell necrosis. *Am J Nephrol* **27**, 416–424.

[42] Kemerink GJ, Liu X, Kieffer D, Ceyssens S, Mortelmans L, Verbruggen AM, Steinmetz ND, Vanderheyden JL, Green AM, and Verbeke K (2003). Safety, biodistribution, and dosimetry of ^{99m}Tc-HYNIC-annexin V, a novel human recombinant annexin V for human application. *J Nucl Med* **44**, 947–952.

[43] Tait JF, Smith C, and Blankenberg FG (2005). Structural requirements for *in vivo* detection of cell death with ^{99m}Tc-annexin V. *J Nucl Med* **46**, 807–815.

[44] Kosaka N, Mitsunaga M, Longmire MR, Choyke PL, and Kobayashi H (2011). Near infrared fluorescence-guided real-time endoscopic detection of peritoneal ovarian cancer nodules using intravenously injected indocyanine green. *Int J Cancer* **129**, 1671–1677.

[45] Sheth RA, Upadhyay R, Stangenberg L, Sheth R, Weissleder R, and Mahmood U (2009). Improved detection of ovarian cancer metastases by intraoperative quantitative fluorescence protease imaging in a pre-clinical model. *Gynecol Oncol* **112**, 616–622.

[46] Bast RC Jr, Hennessy B, and Mills GB (2009). The biology of ovarian cancer: new opportunities for translation. *Nat Rev Cancer* **9**, 415–428.

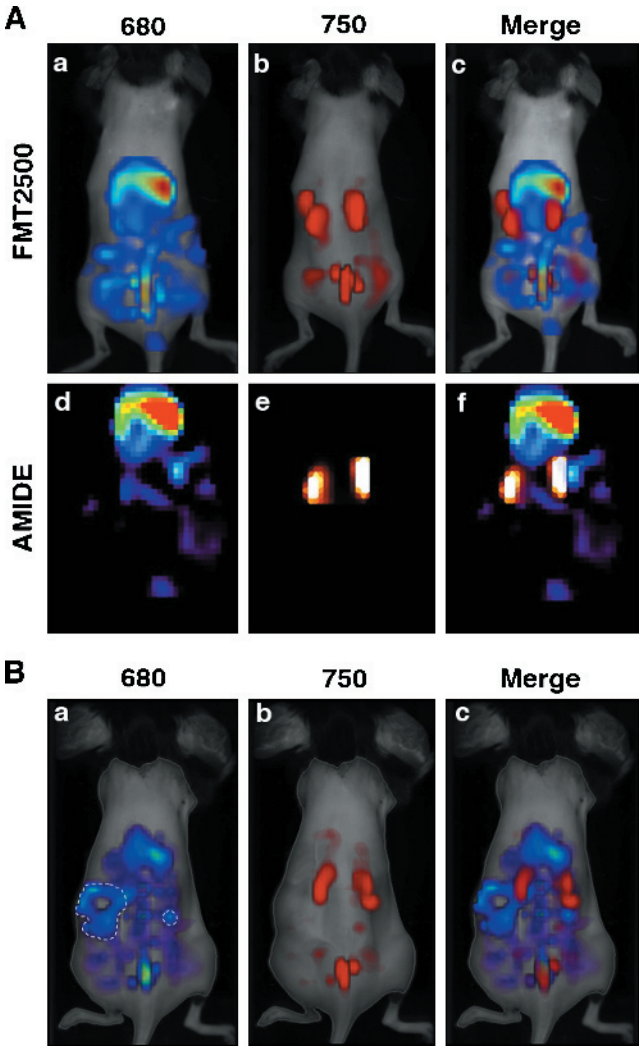

Figure W1. FMT2500 and fused FMT-MR images. (A) A wild-type C57BL/6 mouse was injected with ProSense 680 and AnnexinVivo 750 at 24 and 2 hours before imaging, respectively. Upper panels show the three-dimensional fluorescent images acquired using the (a) 680-nm, (b) 750-nm, and (c) merged 680- and 750-nm channels of the FMT2500 imaging system. Each of the images in a to c were converted using AMIDE and are shown for the 750- and 680-nm channels (d and e) and merged 680- and 750-nm channels (f). (B) Fluorescent images acquired using the (a) 680-nm, (b) 750-nm, and (c) merged 680- and 750-nm channels of the FMT2500 imaging system from a tumor-bearing Tg*MISIIR-TAg* mouse injected with ProSense 680 and AnnexinVivo 750 at 24 and 2 hours before imaging, respectively. The regions corresponding to bilateral tumors are outlined in white (680-nm image, subpanel a).

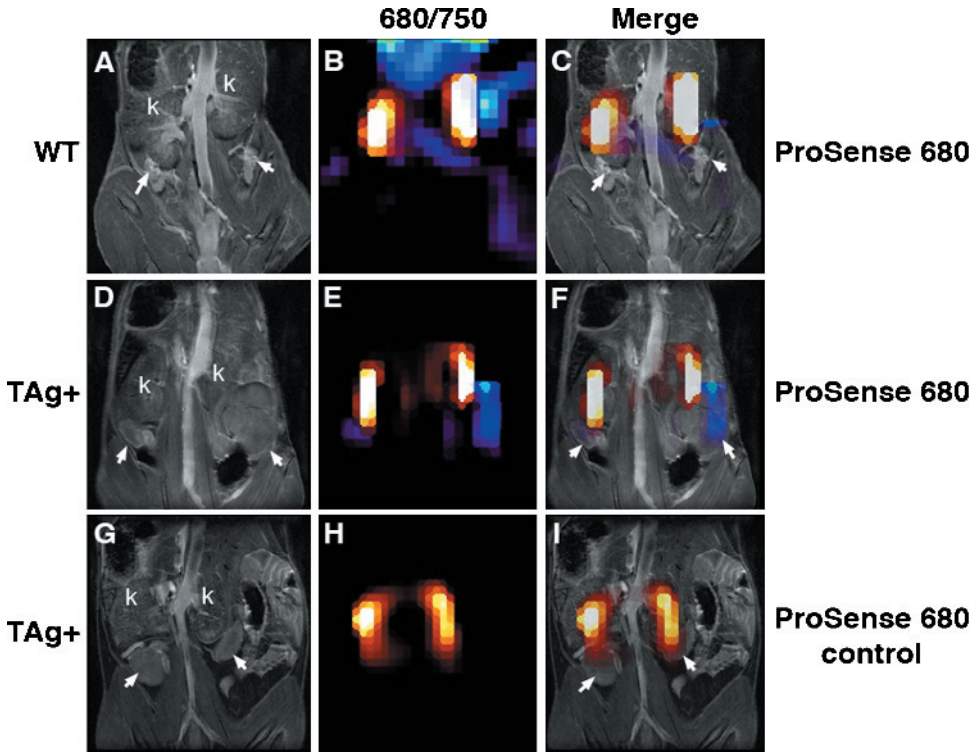

Figure W2. Alignment of MR and FMT images using AnnexinVivo 750. The MR and fluorescent FMT images from wild-type (WT) C57BL/6 and tumor-bearing Tg*MISIIR-TAg* (TAg+) mice injected with ProSense 680 and AnnexinVivo 750 (A-F) or ProSense Control probe and AnnexinVivo 750 (G-I) were aligned using AMIDE. (A, D, and G) MR images showing the ovaries and ovarian tumors (arrows) and kidneys (k). (B, E, and H) Fused images showing merged fluorescent signals detected in the 680- (ProSense or ProSense Control) and 750-nm (AnnexinVivo) channels. (C, F, and I) MR image aligned with both the fluorescent images, showing no probe activation in the normal (wild-type) ovaries (C) or in the ovarian tumors in control probe injected mice (I). Activated probe signal aligns with the ovarian tumors in the ProSense-injected mouse (F).

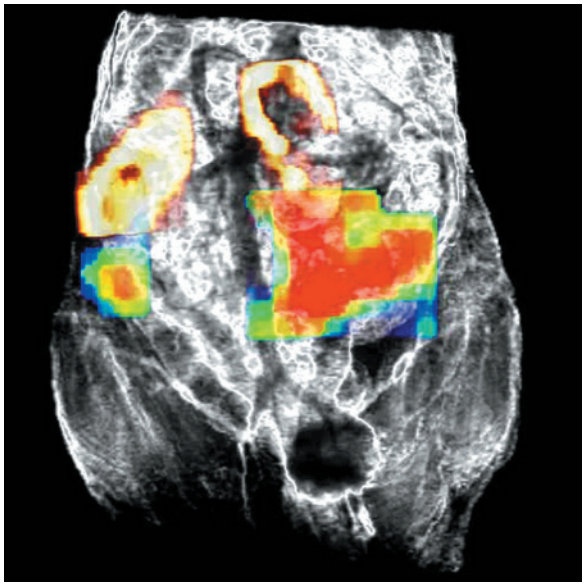

Movie W1. Three-dimensional rendering of images acquired by FMT and MRI. A Tg*MISIIR-TAg* transgenic mouse with bilateral ovarian tumors was injected with ProSense 680 and AnnexinVivo 750 and subjected to FMT and MRI scanning of the entire abdomen. The three-dimensional FMT and MRI data sets were then aligned using AMIDE and rendered to show the anatomic and fluorescent data in three dimensions.